S. B. Choi*
e-mail: seungbok@inha.ac.kr

J. H. Choi

Smart Structures and Systems Laboratory, Department of Mechanical Engineering, Inha University, Incheon 402-751, Korea

Y. S. Lee

M. S. Han

Faculty of Mechanical and Automotive Engineering, Keimyung University, Daegu 704-701, Korea

Vibration Control of an ER Seat Suspension for a Commercial Vehicle

This paper presents a semi-active seat suspension with an electrorheological (ER) fluid damper. A cylindrical ER seat damper is devised on the basis of a Bingham model of an arabic gum-based ER fluid and its field-dependent damping characteristics are empirically evaluated. A semi-active seat suspension is then constructed, and the governing equations of motion are derived by treating the driver mass as a parameter uncertainty. A sliding mode controller, which has inherent robustness to system uncertainties, is formulated to attenuate seat vibration due to external excitations. The controller is then experimentally realized, and controlled responses are presented in both time and frequency domains. In addition, a full-car model consisting of primary, cabin, and seat suspensions is established, and a hardware-in-the-loop simulation is undertaken to demonstrate a practical feasibility of the proposed seat suspension system showing ride comfort quality under various road conditions. [DOI: 10.1115/1.1542639]

1 Introduction

Many commercial vehicles are used for industrial, agricultural, and other transport purposes. The increased number of these vehicles, along with the extended driving hours and the exposure to severe working environments, such as rough road conditions and complex ride behaviors, inevitably results in increased demand for improved ride comfort. Specially, it is observed, based on the measured ride vibration at the driver's seat, that the ride vibration levels of commercial vehicles are 9–16 times higher than those of passenger cars. Moreover, most commercial vehicle drivers are exposed to the ride vibration for 10–20 h/day [1]. The driver's perception of ride comfort is based upon road shock, impact and vibration transmitted through the seat [2]. The ride vibration has a significant influence on the driver's fatigue and safety. Although, improvements in ride comfort have been attempted through appropriate tires, primary and secondary (cabin) suspensions, the suspension at the seat has been considered as a simple and effective option to attenuate vertical vibration. In the majority of commercial vehicles, the seat suspension system is the only mechanism employed to control the transmission of low-frequency and high-amplitude ride vibration. This leads to the study on numerous types of seat suspension systems.

Rakheja et al. [3] constructed a passive seat suspension model and analyzed its dynamic performances. The passive seat suspension system featuring oil dampers provides design simplicity and cost-effectiveness. However, performance limitations such as frequency bandwidth are inevitable. On the other hand, an active seat suspension provides control performance in a wide frequency range. Shimogo et al. [4] constructed an active seat suspension system using a DC servo-motor, which was controlled by an optimal control algorithm. Stein [5] proposed a pneumatic active seat suspension. However, active seat suspension systems require large amount of energy and many other devices such as sensors, controllers, servo-valves, switching modulators, and so forth. In consequence, the actively controlled system is more complex and less reliable. To achieve required performance benefits and overcome drawbacks of active suspension systems, Karnopp et al. [6] developed the concept of a semi-active vibration isolation system. The semi-active isolation system is similar to the passive system in that all suspension elements generate their respective forces passively. However, the damping force generated by the damper can be varied according to a control policy so as to achieve better performance for vibration isolation.

Recently, a very attractive and effective semi-active suspension system featuring ER fluids has been investigated for vibration isolation [7–10]. The suspension system featuring ER fluid dampers has several advantages such as fast response time, continuously controllable damping force, and low energy consumption. Wu and Griffin [11] proposed an ER seat suspension and investigated vibration isolation using many types of on-off control schemes. Brooks [12] proposed a diaphragm-controlled ER seat damper and showed its effectiveness of high damping forces. So far, most of the research on the ER seat damper has been focused on dynamic modeling and field-dependent performance analysis of the ER seat damper itself. Research on vibration isolation of the seat suspension system installed with ER dampers is considerably rare. Moreover, of the research published, none deals with the effectiveness of the ER seat damper for a full-car model subjected to various road conditions. Consequently, the main contribution of this study is to show how the ER seat suspension can attenuate the vibration level at the seat cushion and also to demonstrate the practical feasibility of the ER seat suspension system by showing the ride comfort quality of a full-car model.

In order to accomplish the goals, we first design and manufacture a cylindrical ER seat damper on the basis of the Bingham model of an arabic gum-based ER fluid. Subsequently, a dynamic model for a seat suspension system installed with the ER seat damper is derived and a sliding mode controller is designed to reduce the vibration level due to external excitations. An experimental setup for the ER seat suspension system is established, and controlled responses of vibration isolation are presented in both the time and frequency domains. In addition, a full-car model consisting of primary, cabin, and ER seat suspension systems is derived, and the ride comfort quality is evaluated by adopting the hardware-in-the-loop simulation (HILS) method. The control responses are presented in the frequency domain by comparing with the ISO limit (ISO-2631/1, 1985) [13].

2 Seat Suspension With ER Damper

2.1 Bingham Model of ER Fluid. ER fluids are typically suspensions of conductive particles in the suitable nonconductive

*Corresponding author.

Contributed by the Dynamic Systems and Control Division of THE AMERICAN SOCIETY OF MECHANICAL ENGINEERS for publication in the ASME JOURNAL OF DYNAMIC SYSTEMS, MEASUREMENT, AND CONTROL. Manuscript received by the ASME Dynamic Systems and Control Division, March 1998; final revision, Sept. 2002. Associate Editor: G. Rizzoni.

carrier liquids, which undergo significant instantaneous reversible changes in material characteristics when subjected to applied electric fields [14]. From a mechanics viewpoint, the ER fluid is changed from Newtonian flow in which particles move freely to Bingham behavior in which particles are aligned in a chain and thus have a yield stress upon applying an electric field to the fluid domain. The strength of the electric field which is needed to undergo a phase change from an isotropic material to an anisotropic material is about 1-2 kV/mm. However, due to small current density below about 10 μA/cm^2, power consumption is very low. When the electric field is applied to the ER fluid, the Bingham model of the ER fluid is described by Ginder and Ceccio [15].

$$\tau = \eta\dot{\gamma} + \tau_y(E), \quad \tau_y(E) = \alpha E^{\chi} \tag{1}$$

Here τ is shear stress, η is viscosity, $\dot{\gamma}$ is shear rate and $\tau_y(E)$ is yield stress. As evident from Eq. (1), $\tau_y(E)$ is a function of the electric field of E and exponentially increases with respect to electric field. The parameters of α and χ are characteristic values of a certain ER fluid and can be determined by experiment.

In this study, an arabic gum and silicone oil are chosen as particles and liquid, respectively. The viscosity of the base oil is 0.0027 Pa·s and the weight ratio of the particles to the fluid is 30%. A couette type electroviscometer (Haake VT-500) is employed to obtain the Bingham properties, such as α and χ of the ER fluid. The shear stress is measured with respect to the shear rate at room temperature (25°C) by applying the electric field from 0.5 kV/mm to 5 kV/mm, while the rotational speed increases up to 1000 rpm. Then, from the intercept at zero shear rate, the yield stress $\tau_y(E)$ is obtained to be $35.19E^{1.5}\ Pa$. Here, the unit of E is kV/mm. This experimentally obtained Bingham model is to be incorporated with the seat damper model to analyze field-dependent damping forces.

2.2 Model of ER Damper. Figure 1*a* shows a schematic configuration of the ER seat damper proposed in this study. The ER damper is divided into the upper chamber and lower chamber by a piston, and it is fully filled with the ER fluid. By the motion of piston, the ER fluid flows through the duct between electrodes from one chamber to the other. A voltage drop is produced by a positive voltage connected to the inner cylinder and the negative voltage connected to the outer cylinder. The gas chamber acts as accumulator of the ER fluid induced by the motion of the piston, and thus preventing cavitation. If no electric field is applied, the ER damper produces the damping force caused by the fluid resistance. However, if a certain level of the electric field is supplied to the ER damper, the ER damper produces an additional damping force based on the yield stress of the ER fluid. This damping force of the ER damper can be continuously controlled by controlling the intensity of the electric field. In order to simplify the analysis of the ER damper, it is assumed that the ER fluid is an incompressible fluid. In the absence of the electric field the flow resistance through the duct between the electrodes is given by

$$R_e = \frac{12\eta L}{bh^3} \tag{2}$$

where L is the electrode length, b is the electrode width, and h is the electrode gap. It is noted that Eq. (2) is valid for only fully-developed steady laminar flow. It does not account for the dynamic effect induced by a sinusoidal flow. Moreover, the effect of the fluid inertia on the damping force is neglected since the operating frequency range of the proposed ER seat damper is relatively low and the amount of the fluid mass between electrode gaps is little. By assuming that the gas usually does not exchange much heat with its surroundings, the compliance of the gas C_g can be expressed by

$$C_g = \frac{V_0}{P_0 n} \tag{3}$$

where V_0 and P_0 are the initial volume and pressure of the gas, respectively. The variable of n is the ratio of the specific heat ratio. On the other hand, the pressure drop due to the electric field is given by

$$\Delta P_{ER} = 2\frac{L}{h}\tau_y(E) = 2\frac{L}{h}\alpha E^{\chi} \tag{4}$$

Now, from the bond graph model shown in Fig. 1*b*, the governing equations of motion of the ER seat damper can be directly obtained as follows.

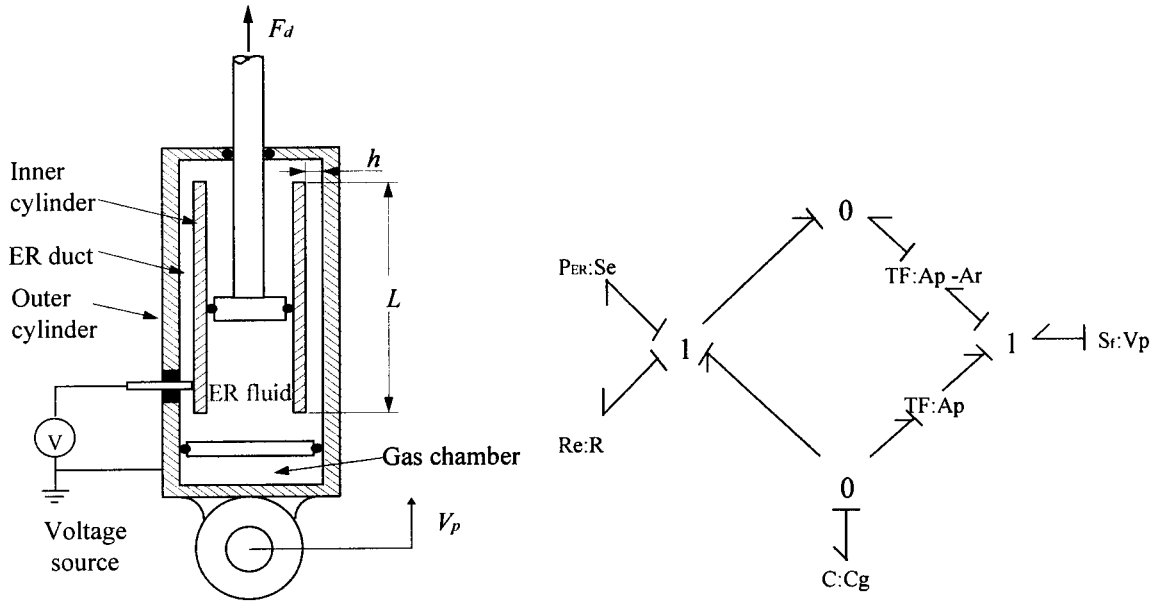

(*a*) schematic diagram (*b*) bond graph model

Fig. 1 Proposed ER seat damper

$$\dot{q}_d = -A_r V_p \tag{5}$$

$$F_d = -\frac{A_r}{C_g} q_d + (A_p - A_r)^2 R_e V_p + (A_p - A_r) sgn(V_p) \Delta P_{ER} \tag{6}$$

Here, q_d is the fluid volume of the lower chamber, F_d is damping force, V_p is the excitation velocity, A_r is area of piston rod, A_p is area of the piston, and $sgn(n)$ is a signum function. The damping force given by Eq. (6) can be rewritten by

$$F_d = k_e X_p + c_e V_p + F_{ER} \tag{7}$$

where, X_p is the excitation displacement, k_e is the effective stiffness due to the gas pressure, c_e is the effective damping due to the viscosity, and F_{ER} is the damping force which is tunable as a function of electric field. This controllable damping force F_{ER} can be given by

$$F_{ER} = 2(A_p - A_r)\frac{L}{h}\alpha E^x sgn(V_p) \tag{8}$$

The size and the level of required damping force adopted in this work are chosen on the basis of conventional passive oil damper for a commercial truck. The governing equation (7) is evaluated with respect to the electric field in order to determine design parameters such as the electrode gap. The designed ER seat damper has the following specifications: electrode gap size, 1 mm; electrode length, 120 mm; diameter of piston rod, 11 mm; diameter of piston, 30 mm; and diameter of inner cylinder, 36 mm. Figure 2*a* shows a photograph of the ER seat damper manufactured in this study, and Fig. 2*b* presents the measured damping forces with respect to the piston velocity. The piston velocity is changed by increasing the excitation frequency from 0.5 Hz to 3.5 Hz, where the excitation amplitude is maintained to be constant by 20 mm. The experimental setup and procedures for the measurement of the damping forces are well described in Choi et al. [10], and hence omitted. As expected, the damping force increases as the electric field increases. This indicates that a certain desired damping force within the range of 0–5 kV/mm can be achieved by controlling the electric field regardless of the piston velocity. This is a salient feature of the ER seat damper.

2.3 Model of ER Seat Suspension System. Figure 3*a* shows a mathematical model of the proposed semi-active suspension system featuring the ER seat damper. The governing equations of motion of the ER seat suspension can be obtained as follows:

$$\begin{aligned} m_1\ddot{q}_1 &= -c_1(\dot{q}_1 - \dot{q}_0) - k_1(q_1 - q_0) + c_2(\dot{q}_2 - \dot{q}_1) \\ &\quad + k_2(q_2 - q_1) - u \\ m_2\ddot{q}_2 &= -c_2(\dot{q}_2 - \dot{q}_1) - k_2(q_2 - q_1) \end{aligned} \tag{9}$$

where, m_1 and m_2 represents the mass of the seat suspension and the mass of the driver, respectively. k_1 and c_1 denote spring and damping constants of the seat suspension, while k_2 and c_2 stand for stiffness and damping constants of the seat cushion. It is noted that the spring constant k_1 is equal to sum of the spring constant of the suspension spring (k_s) and k_e in Eq. (7). The damping constant c_1 is equal to c_e in Eq. (7). The variable u represents the controllable damping force F_{ER}. By defining the state vector as $X = [q_1 \;\; q_2 \;\; \dot{q}_1 \;\; \dot{q}_2]^T$, we obtain the following state equation.

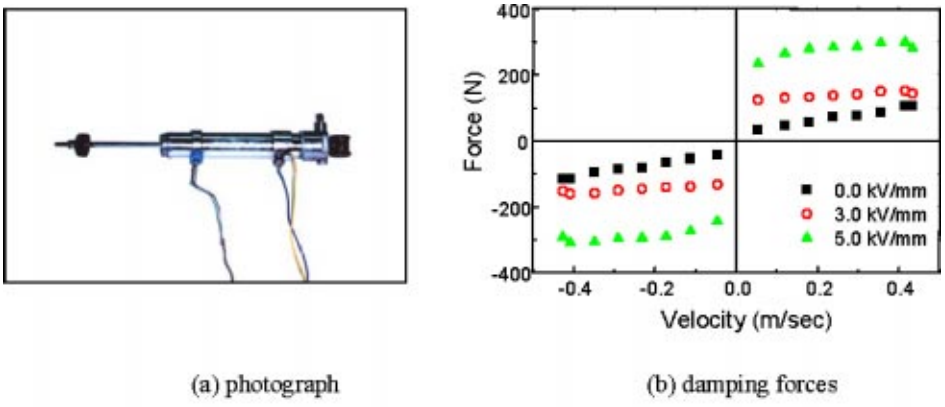

Fig. 2 Photograph and damping forces of the proposed ER seat damper

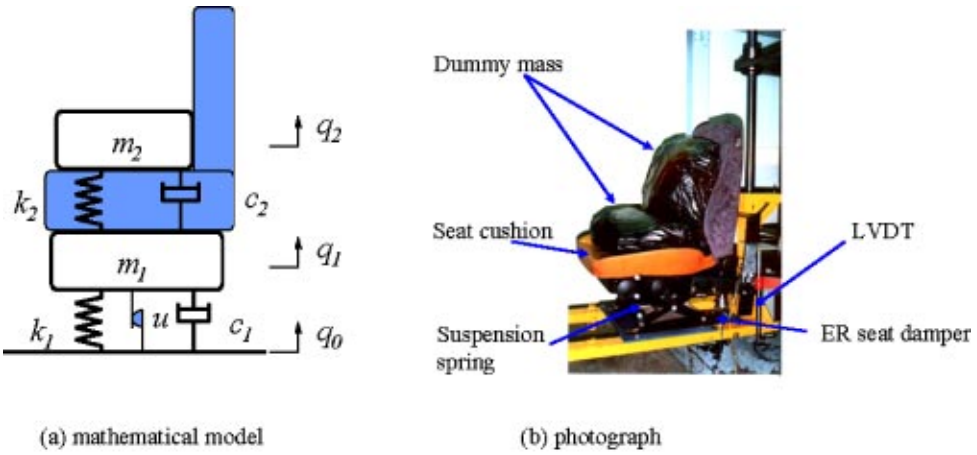

Fig. 3 Proposed ER seat suspension system

$$\dot{X}=AX+Bu+D \tag{10}$$

where,

$$A=\begin{bmatrix} 0 & 0 & 1 & 0 \\ 0 & 0 & 0 & 1 \\ -\frac{k_1+k_2}{m_1} & \frac{k_2}{m_1} & -\frac{c_1+c_2}{m_1} & \frac{c_2}{m_1} \\ \frac{k_2}{m_2} & -\frac{k_2}{m_2} & \frac{c_2}{m_2} & -\frac{c_2}{m_2} \end{bmatrix},$$

$$B=\begin{bmatrix} 0 \\ 0 \\ -\frac{1}{m_1} \\ 0 \end{bmatrix}, \quad D=\begin{bmatrix} 0 \\ 0 \\ \frac{c_1}{m_1}\dot{q}_0+\frac{k_1}{m_1}q_0 \\ 0 \end{bmatrix}$$

In practice, the mass of the driver m_2 may be varied due to riders with different masses. Thus, we consider that a parameter perturbation of the driver mass m_2 exists in the system. From empirical data, the possible bound of the uncertain system parameter can be defined by

$$m_2=m_{20}+\Delta m, \quad |\Delta m|\leqslant 0.5m_{20} \tag{11}$$

Here, m_{20} represents the nominal part and Δm the uncertain part. By assuming that so-called matching condition [16] is satisfied, this uncertainty can be expressed by

$$\frac{1}{m_{20}+\Delta m}=\frac{1}{m_{20}}(1+\gamma_u), \quad |\gamma_u|\leqslant\phi<1 \tag{12}$$

where, γ_u and ϕ are constant values. The matching condition physically implies that the uncertain part Δm cannot have an arbitrarily large perturbation. Substituting Eq. (12) into Eq. (10), the state space equation with the parameter uncertainty is obtained as follows.

$$\dot{X}=(A_0+\Delta A)X+Bu+D \tag{13}$$

Here, A_0 and ΔA are the nominal and uncertain part of the system matrix, respectively.

3 Controller Design

In this study, a sliding mode controller which has inherent robustness to system uncertainties is adopted to suppress the vibration level. As a first step for designing the sliding mode controller, we define the following sliding surface.

$$S(X)=CX=0 \tag{14}$$

where, C is surface gradient to be determined so that the sliding surface itself is asymptotically stable. In order to determine C the eigenvector W associated with desired eigenvalues can be obtained by Dorling and Zinober [17] and El-ghezawi et al. [18]

$$A_0W-WJ=BN \tag{15}$$

where, J is Jordan-block form associated with desired eigenvalues and N is an arbitrary matrix chosen to provide linear combinations of the column B. Then the surface gradient C is defined by the generalized inverse of B which is augmented to the eigenvector W. The desired eigenvalues of $-10\pm 10i$, -60 are chosen, and hence C is obtained by $[-1137.63,\ 739.726,\ -20,\ -126.279]$.

Now in order to formulate the sliding mode controller, which guarantees robust stability and high performance for the uncertain system parameter, we assume that each uncertain element of ΔA is to be bounded as $|\delta a_{ij}|\leqslant\overline{a}_{ij}<\infty$. Thus, we define the matrix $\overline{A}$ in which all uncertain elements δa_{ij} are replaced by $\overline{a}_{ij}$. In this study, the values for $\overline{a}_{ij}$ are specified as $\overline{a}_{i1}=\overline{a}_{i2}=\overline{a}_{i3}=\overline{a}_{i4}=0(i=1,2,3)$, $\overline{a}_{41}=82.29$, $\overline{a}_{42}=-82.29$, $\overline{a}_{43}=1.53$, and $\overline{a}_{44}=-1.53$. Consequently, we can formulate the following sliding mode controller which satisfies the sliding mode condition $S(X)\dot{S}(X)<0$.

$$u=-\frac{1}{1-\phi}(CB)^{-1}[\{|CA_0X|+|C\overline{A}X|\}sgn(S)+Knsgn(S)] \tag{16}$$

Here $K=C\overline{D}$, $\overline{D}=[0,\ 0,\ (k_1/m_1)\psi_1+(c_1/m_1)\psi_2,\ 0]^T$, $\psi_1\geqslant|q_0|$, and $\psi_2\geqslant|\dot{q}_0|$. Then we can show that the uncertain system given by Eq. (13) with the controller u given by Eq. (16) satisfies the sliding mode condition as follows:

$$\begin{aligned} S(X)\dot{S}(X)&=S(X)[C\{(A_0+\Delta A)X+Bu+D\}] \\ &=S(X)\left[\left\{CA_0X-\frac{1}{1-\phi}\left|CA_0X\right|sgn(s)\right\}\right. \\ &\quad+\left\{C\Delta AX-\frac{1}{1-\phi}\left|C\overline{A}X\right|sgn(s)\right\} \\ &\quad\left.+\left\{CD-\frac{1}{1-\phi}Ksgn(s)\right\}\right]<0 \end{aligned} \tag{17}$$

Since the controller u given by Eq. (16) includes the sign function, undesirable chattering may occur during control action. This may be attenuated by replacing the sign function by the saturation function with appropriate boundary layer thickness ε. The control input u is designed in an active actuating manner. However, the proposed ER seat suspension is a semi-active. Thus, the control input should be applied according to the following actuating condition.

$$\begin{aligned} &If\ \ u\cdot sgn(\dot{q}_1-\dot{q}_0)>0, \quad u=u \\ &If\ \ u\cdot sgn(\dot{q}_1-\dot{q}_0)<0, \quad u=0 \end{aligned} \tag{18}$$

This condition physically implies that the actuating of the controller u only assures the increment of energy dissipation. Once the control input u is determined, the control electric field to be applied to the ER seat damper is obtained from Eq. (8) as follows.

$$E=\left[\frac{u}{(A_p-A_r)}\cdot\left(\frac{h}{2L\alpha}\right)\right]^{\frac{1}{\lambda}} \tag{19}$$

In this work, the control parameters for the sliding mode controller are chosen as follows: $\phi=0.53$, $K=35.0$, and $\varepsilon=0.18$

4 Seat Suspension Test

4.1 Parameter Identification. The suspension model requires the material properties of the seat spring and the seat cushion. The suspension spring constant can be obtained from the force-deflection relationship. Figure 4*a* shows the measured force-deflection characteristic of the suspension spring. From the curve fitting, the suspension spring constant (k_s) is evaluated by 6300 N/m. The damping and spring constants of the seat cushion are evaluated via dynamic test using sinusoidal displacement excitation. The measured force-displacement relationship is shown in Fig. 4*b*. From the measured curve, it is known that the curve is the form of Lissajous diagram from which the equivalent viscous damping coefficient of the seat cushion can be evaluated as follows [19].

$$c_2=\frac{Area\ \ within\ \ Lissajous\ \ curve}{\pi\ (2\pi f)\ X^2} \tag{20}$$

where, f is excitation frequency and X is the peak to peak displacement. Consequently, from the slope of the curve fit, the cushion spring constant (k_2) is determined to be 8228.78 N/m. And from the formula given by Eq. (20), the cushion damping constant

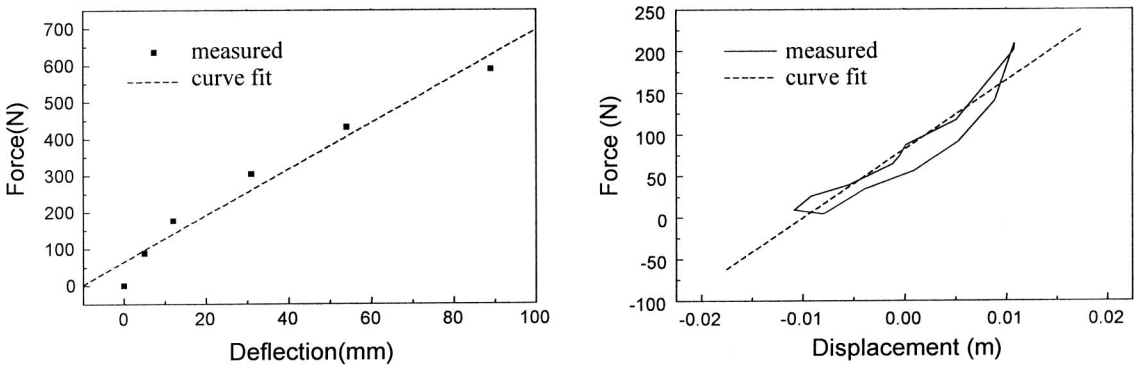

(*a*) suspension spring (*b*) seat cushion

Fig. 4 Parameter identification for seat suspension and seat cushion

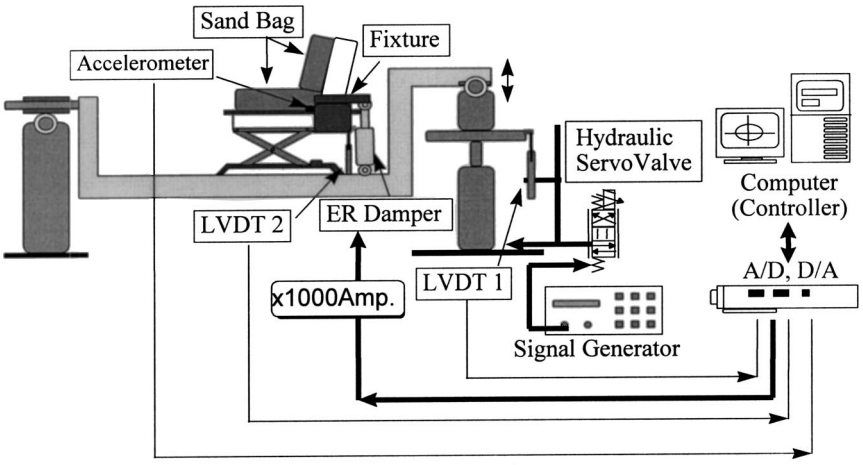

Fig. 5 Experimental apparatus for seat suspension test

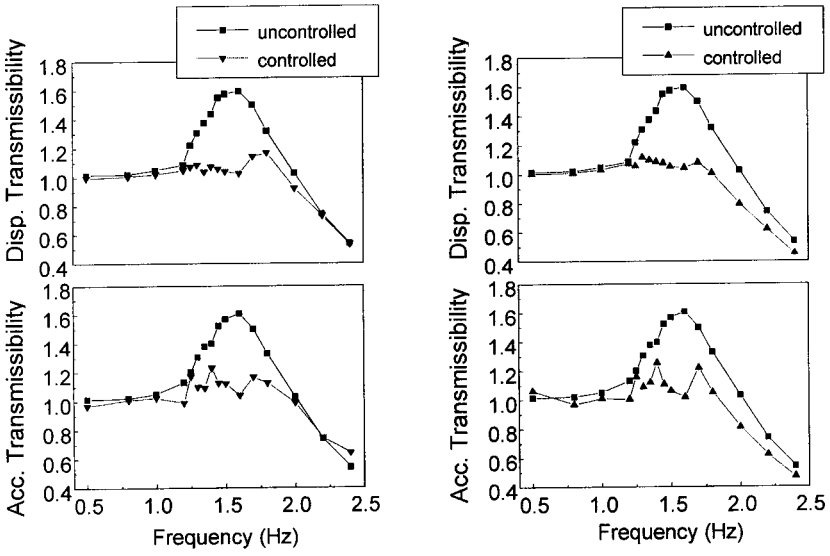

(*a*) without mass uncertainty (*b*) with mass uncertainty

Fig. 6 Control responses of ER seat suspension system in frequency domain

(c_2) is determined to be 152.8 Ns/m. The parameters k_e and c_1 are available from the characteristics of the ER seat damper. The other system parameters for the ER seat suspension system are given as follows: seat frame mass (m_1), 20 kg; driver mass (m_2), 50 kg; suspension damping (c_1), 1429.84 Ns/m; and gas spring constant (k_e), 1114.86 N/m.

4.2 Test Results and Discussions. An experimental apparatus is established as shown in Fig. 5 to evaluate the effectiveness of vibration isolation of the proposed suspension system. The seat suspension is mounted on the vibration platform, and two sandbags accounting for the driver mass are loaded on the seat. The acceleration from the accelerometer mounted on the seat cushion and vertical displacement from the LVDT2 are measured and fed back to the sliding mode controller. The control electric field determined in the controller is provided to the ER seat damper via the D/A converter and high voltage amplifier. Figures 6 and 7 present uncontrolled and controlled responses in frequency and time domains, respectively. The uncontrolled one is obtained in the absence of the electric field without activating the controller. It is seen that the suspension system has the natural frequency of 1.6 Hz without control voltage. Both the vertical displacement and acceleration transmissibility are high at resonance. However, by employing the control electric field determined from the sliding mode controller, the peak is substantially reduced even in the presence of the mass uncertainty. The parameter uncertainty of Δm is imposed by 15 kg. The control result directly implies the effectiveness and robustness of the proposed control system. In Fig. 7, we see that the vibration level at the resonance excitation is reduced by applying the control voltage, as expected. In addition, it is observed that the control electric field is applied according to the imposed actuating condition given by Eq. (18). In order to demonstrate a practical feasibility of the ER seat suspension system, a durability of the control performance is tested and presented in Fig. 8. The seat is excited with the frequency of 1.6 Hz, which is the system's natural frequency, and the magnitude of ± 20 mm. It is clearly seen that the displacement increases as time goes on without the controller. This arises from the fact that as time increases the operating temperature of the ER fluid increases. This change in operating temperature results in a change in the properties of the ER fluid such as the viscosity. However, the

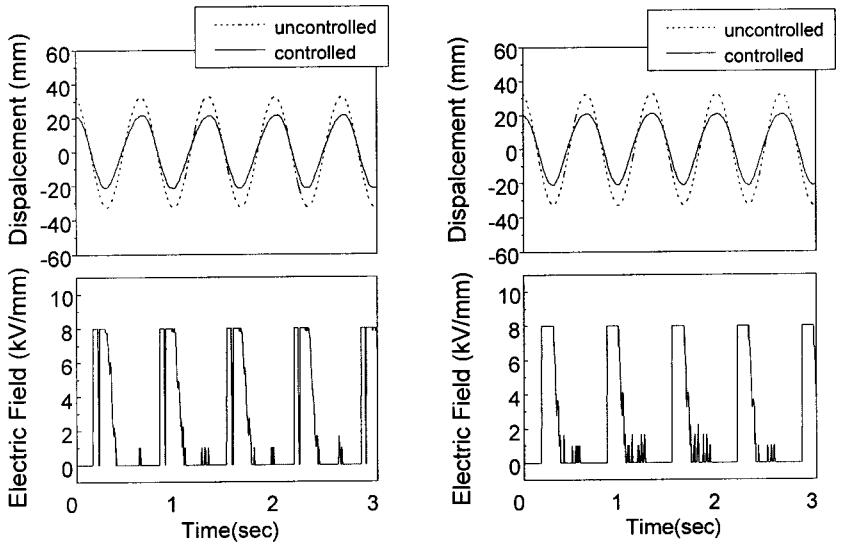

(a) without mass uncertainty (b) with mass uncertainty

Fig. 7 Control responses of ER seat suspension system in time domain

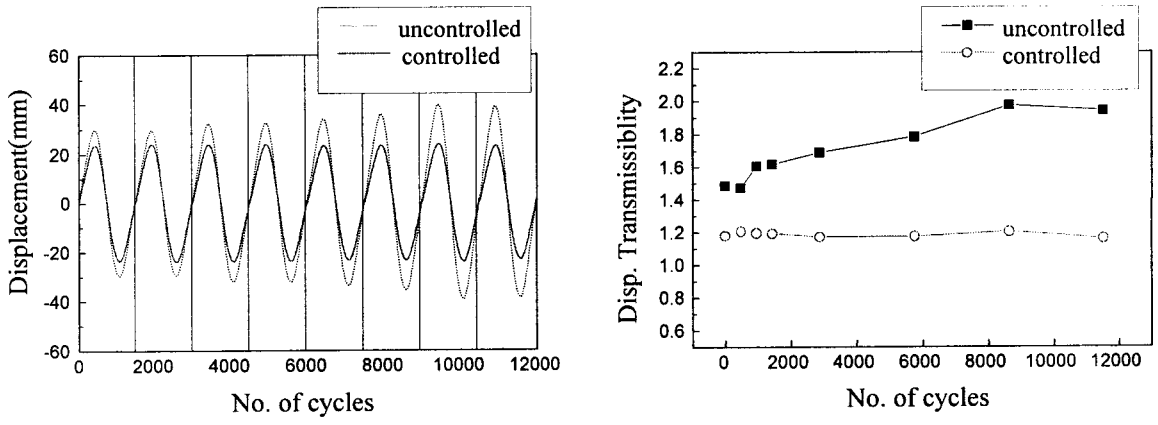

(a) time history (b) transmissibility at 1.6Hz

Fig. 8 Control durability of the ER seat suspension system

degradation of the damping performance is not observed in the controlled case. This advocates the robustness and durability of the proposed control system under variable operating conditions.

5 Full-Car Responses via Hardware-in-the-Loop Simulation

5.1 Dynamic Model. A full-car model consisting of primary, cabin and seat suspension systems is shown in Fig. 9. The excitation input from the road is transmitted through to the cabin floor. This causes undesirable vibrations on the driver. By defining the state variables as $z=[q_{p1}\ \dot{q}_{p1}\ q_{p2}\ \dot{q}_{p2}\ q_{bc}\ \dot{q}_{bc}\ \phi\ \dot{\phi}\ q_{cc}\ \dot{q}_{cc}\ \theta\ \dot{\theta}]^T$, we derive the following equations of motion:

$$\dot{z}_1=z_2,\quad \dot{z}_2=\frac{1}{m_{p1}}(f_1-f_2)$$

$$\dot{z}_3=z_4,\quad \dot{z}_4=\frac{1}{m_{p2}}(f_3-f_4)$$

$$\dot{z}_5=z_6,\quad \dot{z}_6=\frac{1}{m_b}(f_2+f_4)$$

$$\dot{z}_7=z_8,\quad \dot{z}_8=\frac{1}{J_b}(af_2-bf_4)$$

$$\dot{z}_9=z_{10},\quad \dot{z}_{10}=\frac{1}{m_c}(f_5+f_6)$$

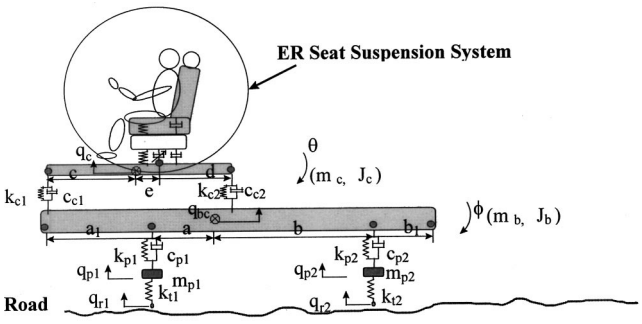

Fig. 9 Dynamic model of a full-car suspension system

$$\dot{z}_{11}=z_{12},\quad \dot{z}_{12}=\frac{1}{J_c}(cf_5-df_6) \tag{21}$$

where,

$$f_1=k_{t1}(q_{r1}-z_1)$$

$$f_2=k_{p1}[z_1-(z_5+az_7)]+c_{p1}[z_2-(z_6+az_8)]$$

$$f_3=k_{t2}(q_{r2}-z_3)$$

$$f_4=k_{p2}[z_3-(z_5-bz_7)]+c_{p2}[z_4-(z_6-bz_8)]$$

$$f_5=k_{c1}[(z_5+a_1z_7)-(z_9+cz_{11})]+c_{c1}[(z_6+a_1z_8)-(z_{10}+cz_{12})]$$

$$f_6=k_{c2}[(z_5+b_1z_7)-(z_9-dz_{11})]+c_{c2}[(z_6+b_1z_8)-(z_{10}-dz_{12})] \tag{22}$$

The governing equations are to be solved by a digital computer in real-time. It is also noted that the cabin floor displacement is represented by $q_0=z_9-ez_{11}$. This cabin floor input is to be applied to the ER seat suspension system via hydraulic servo-actuator.

5.2 HILS Results and Discussions. From a practical point of view, the proposed ER seat suspension system should be installed on a full car, and its effectiveness for the ride quality needs to be tested with respect to various road conditions. However, it is very expensive to completely build the entire full-car system with hardware from the start. Therefore, we adopt a hardware-in-the-loop simulation (HILS) in which a full-car system model consisting of the primary and cabin suspension systems is incorporated with actual hardware of the proposed ER seat suspension system. Figure 10 presents a schematic configuration of the HILS method. In the real-time simulation, the road and driving conditions are adopted for the conventional COE (cab over engine) type commercial vehicle model. The system parameters of this model are listed in Table 1. The full-car model of a commercial vehicle in the computer system is to be excited from prescribed road profiles. The cabin floor displacement is calculated and then the displacement signal is converted to the hydraulic control unit for controlling the road input to the platform. When the vibration is transmitted to the ER seat suspension system, the signals, which are acquired from the LVDT2 and accelerometer, are converted to digital signals via the A/D converter. The sliding mode controller is then activated to reduce the vibration level at the seat cushion.

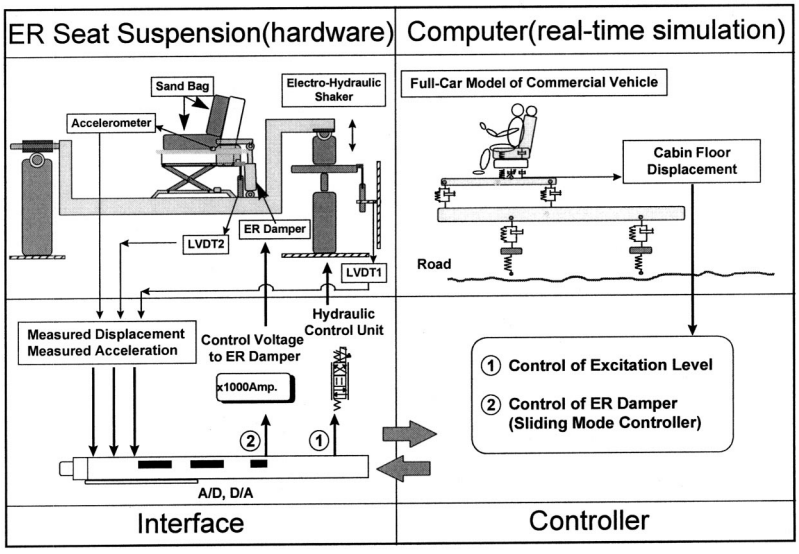

Fig. 10 System configuration for HILS

Table 1 System parameters of the full-car model

Parameter	Value	Parameter	Value
unsprung mass 1 (m_{p1})	803 kg	primary suspension damping 1 (c_{p1})	33000 Ns/m
unsprung mass 2 (m_{p2})	1503 kg	primary suspension damping 2 (c_{p2})	33000 Ns/m
car body mass (m_b)	3450 kg	cabin suspension damping 1 (c_{c1})	5073.5 Ns/m
cabin mass (m_c)	950 kg	cabin suspension damping 2 (c_{c2})	5073.5 Ns/m
car body inertia (J_b)	9500 kg·m^2	from car C. G. to steer axle (a)	1.15 m
cabin inertia (J_c)	800 kg·m^2	from car C. G. to rear steer axle (b)	2.8 m
tire stiffness 1 (k_{t1})	4,000,000 N/m	from car C. G. to front end (a_1)	1.8 m
tire stiffness 2 (k_{t2})	4,000,000 N/m	from car C. G. to rear end (b_1)	3.4 m
primary suspension stiffness 1 (k_{p1})	40,000 N/m	from cab C. G. to cabin front end (c)	0.85 m
primary suspension stiffness 2 (k_{p2})	40,000 N/m	from cab C. G. to cabin rear end (d)	1.15 m
cabin suspension stiffness 1 (k_{c1})	63,757.5 N/m	from cab C. G. to seat suspension (e)	0.01 m
cabin suspension stiffness 2 (k_{c2})	63,757.5 N/m		

The experimentally measured vibration levels (displacement and acceleration) are integrated with the excitation magnitude and control logic in real-time fashion.

Figure 11 presents frequency responses of the proposed control system under two different types of road conditions. The road profile for the HILS is generated by using the homogeneous Gaussian random process [20]. For the asphalt road, the road roughness factor, covariance, and vehicle velocity are chosen by 0.15 m^{-1}, 9 mm^2, and 20 m/s, respectively. The corresponding values for the paved road are 0.45 m^{-1}, 300 mm^2, and 7 m/s. As shown in Fig. 11, the frequency responses are compared with ISO 2631FDP-1 hr limit [13], which specifies comfort boundary of human beings for acceleration power spectral density (PSD). The PSD values of acceleration are measured from the low-frequency accelerometer positioned on the seat cushion. It is clearly observed from Fig. 11 that the acceleration level of the uncontrolled case exceeds the ISO limit in the neighborhood of the first mode natural frequency. However, using the sliding mode controller the performance of the ER seat suspension is substantially improved to satisfy ISO limit over a wide range of frequencies. It is also seen that the proposed control system is very effective when subjected to uncertainties in the mass. This implies that we can achieve the control robustness using the sliding mode controller.

6 Conclusions

An ER seat suspension system was proposed for commercial vehicles and its control performances were investigated. After manufacturing a cylindrical-type ER seat damper, field-dependent damping forces were tested. A sliding mode controller was then designed by considering the driver mass as the parameter uncertainty to reduce the vibration level at the seat cushion. Favorable vibration isolations have been achieved by realizing the controller in the presence of the uncertainty. In addition, the hardware-in-the-loop simulation was undertaken to demonstrate the practical feasibility of the proposed system. The vibration level represented

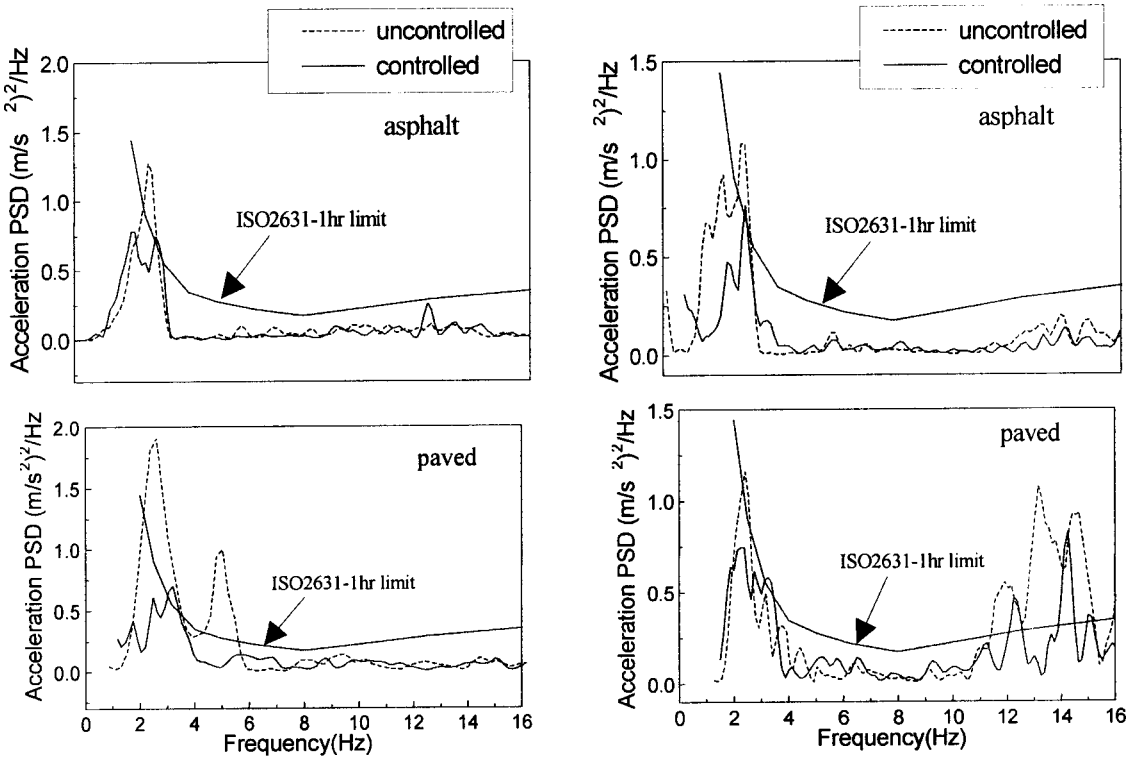

(a) without mass uncertainty (b) with mass uncertainty

Fig. 11 Frequency responses on the seat cushion via HILS

by acceleration power spectral density at the seat cushion was significantly reduced to satisfy ISO limit by adopting the sliding mode controller. The results presented in this work are quite self-explanatory justifying that the ER seat suspension system is very effective for vibration isolation. A comparative work between the proposed ER seat suspension system and conventional passive or semiactive seat suspension needs to be undertaken in the near future.

References

[1] Queslati, F., and Sankar, S., 1992, ''Performance of a Fail-Safe Active Suspension With Limited State Feedback for Improved Ride Quality and Reduced Pavement Loading in Heavy Vehicles,'' *SAE Paper,* No. 922474, pp. 796–804.

[2] Reynolds, H. M., 1993, *Automotive Ergonomics,* Taylor and Francis Ltd, London, pp. 99–116.

[3] Rakheja, S., Afework, Y., and Sankar, S., 1994, ''An Analytical and Experimental Investigation of the Driver-Seat-Suspension System,'' Veh. Syst. Dyn., **23**, pp. 501–524.

[4] Shimogo, T., Oshinoya, Y., and Shinjyo, H., 1996, ''Active Suspension of Truck Seat,'' JSME **62**, pp. 192–198.

[5] Stein, G. J., 1997, ''A Driver's Seat with Active Suspension of Electro-pneumatic Type,'' J. Vibr. Acoust., **119**, pp. 230–235.

[6] Karnopp, D., Crosby, M. J., and Harwood, R. A., 1974, ''Vibration Control Using Semi-active Force Generators,'' ASME J. Eng. Ind., **96**(2), pp. 619–626.

[7] Morishita, S., Mitsui, J., and Kuroda, Y., 1990, ''Controllable Shock Absorber as an Application of Electro-rheological Fluid,'' JSME **56**, pp. 78–84.0

[8] Petek, N. K., 1995, ''Demonstration of an Automotive Semi-active Suspension Using Electrorheological Fluid.'' *SAE Paper,* No. 950586.

[9] Sturk, M., Wu, X. M., and Wong, J. Y., 1995, ''Development and Evaluation of a High Voltage Supply Unit for Electrorheological Fluid Dampers,'' Veh. Syst. Dyn., **24**, pp. 101–121.

[10] Choi, S. B., Choi, Y. T., Chang, E. G., Han, S. J., and Kim, C. S., 1998, ''Control Characteristics of a Continuously Variable ER Damper,'' Mechatronics, **8**, pp. 143–161.

[11] Wu, X., and Griffin, M. J., 1997, ''A Semi-active Control Policy to Reduce the Occurrence and Severity of End-stop Impacts in a Suspension Seat with an Electrorheological Fluid Damper,'' J. Vibr. Acoust., **203**(5), pp. 781–793.

[12] Brooks. D. A., 1997, ''High Performance Damping Using Electro-Rheological Fluids,'' *Proc. of Int. Conf. on ERF, MRS and Their Applications*, Yamagata, Japan, pp. 250–251.

[13] International Standard Organization ISO-2631/1, 1985, ''Evaluation of Human Exposure to Whole-Body Vibration, Part 1: General Requirements.''

[14] Winslow, W. M., 1949, ''Induced Fibration Suspension,'' J. Appl. Phys., **20**, pp. 1137–1140.

[15] Ginder, J. M., and Ceccio, S. L., 1995, ''The Effect of Electrical Transients on the Shear Stresses in Electrorheological Fluids,'' J. Rheol., **39**, pp. 211–234.

[16] Leitmann, G., 1981, ''On the Efficiency of Nonlinear Control in Uncertain Linear Systems,'' ASME J. Dyn. Syst., Meas., Control, **102**, pp. 95–102.

[17] Dorling, C. M., and Zinober, A. S. I., 1986, ''Two Approaches to Hyperplane Design in Multivariable Variable Structure Control Systems,'' International Journal of Control, **44**(1), pp. 65–82.

[18] El-ghezawi, O. M. E., Zinober, A. S. I., and Billings, S. A., 1983, ''Analysis and Design of Variable Structure Systems using a Geometric Approach,'' Int. J. Control, **38**(3), pp. 657–671.

[19] Gouw, G. J., Rakheja, S., Sankar, S., and Afework, Y., 1990, ''Increased Comfort and Safety of Drivers of Off-highway Vehicles using Optimal Seat Suspension,'' *SAE Paper,* No. 901646.

[20] Nigam, N. C., Narayanan, S., 1994, *Applications of Random Vibrations*, Springer-Verlag, pp. 219–292.